

# Transformer-based Modeling of Physical Systems: Improved Latent Representations

Arnaud Pannatier<sup>1,2</sup> Kyle Matoba<sup>1,2</sup> François Fleuret<sup>3</sup>

## Abstract

Many phenomena from physics and engineering require highly flexible models, and have ample data with which to fit. However, this data is often irregularly sampled, and cannot be processed as it is by standard deep learning architecture. We propose a transformer-based model for forecasting physical processes at arbitrary spatial points given information on a related process at possibly different points. This architecture is particularly well-suited for high-altitude wind forecasting, as it can effectively leverage large volumes of data recorded along plane trajectories, which are sparse in space.

We test at different scales for two different dynamical systems previously studied in the literature: the Poisson equation and Darcy Flow equation. In both cases, our transformer-based model outperforms alternative methods. We hypothesize that this superior performance is due to a more flexible latent representation. To support this hypothesis, we design a simple synthetic experiment to show that the latent representation of the other models suffers from excessive bottlenecks that is, in some cases, preventing the efficient use of the information and slowing training.

## 1. Introduction

Deep learning (DL) has emerged as a powerful tool for dynamical system modeling in recent years, leveraging vast amounts of data available in ways that traditional solvers cannot. This has led to a growing reliance on DL models in weather forecasting, with state-of-the-art results in precipitation nowcasting (Suman et al., 2021; Shi et al., 2017) and performance on par with traditional partial differential

equation (PDE) solvers in medium-term forecasting (Lam et al., 2022). However, these applications are currently limited to data represented as images or on regular spherical grids, where standard models such as convolutional networks or graph neural networks are used. In contrast, various real-world applications, such as wind nowcasting based on flight data, require special architectures to process irregularly sampled datasets.

Air traffic control (ATC) requires reliable weather forecasts to manage airspace efficiently. This is particularly true for wind conditions, as planes are highly sensitive to wind and deviations from the initial flight plan can be costly and pose safety hazards. DL models are a viable candidate to produce reliable wind forecasts as a large amount of data is collected from airplanes that broadcast wind speed measurements with a recording frequency of around four seconds. To effectively model wind nowcasting using data collected from airplanes, we require a model that can encode recent measurements. This encoding should be done in a permutation-invariant way, as the order of contemporary measurements in a “context” of recent data should not impact the prediction. The model must also be able to decode anywhere in space, as we aim to predict wind conditions at future locations of the airplane, based on past measurements taken by that specific airplane or neighboring ones. This decoding should be permutation-equivariant, i.e., a permutation of the target position should permute the outputs accordingly.

To meet these requirements, we introduce a Transformer-based model (TFS) and compare it to two different baselines: Conditional Neural Processes (CNP) (Garnelo et al., 2018) and Graph Element Networks (GEN) (Alet et al., 2019). These models all have the properties described above, but they differ in the way they represent measurements in the latent space. CNP models use a single vector as a summary of encoded measures, while GEN models map the context to a graph based on their distance to its nodes. TFS keep one latent representation per encoded measurement so that the decoder can access them efficiently for forecasting. This latent representation is better and is the reason for the use of transformers. We show that due to that architectural choice, both baselines fail to retrieve information present in the context they condition on.

<sup>1</sup>Idiap Research Institute, Martigny, Switzerland <sup>2</sup>Computer Science Department, École Polytechnique Fédérale de Lausanne, Lausanne, Switzerland <sup>3</sup>Computer Science Department, Université de Genève, Geneva, Switzerland. Correspondence to: Arnaud Pannatier <arnaud.pannatier@idiap.ch>.

To evaluate the effectiveness of these models for dynamical systems, we conducted experiments on real data from high-altitude wind nowcasting tasks as well as two synthetic tasks: Poisson equation (Alet et al., 2019) and Darcy Flow equation (Li et al., 2021). We conducted several other ablations to show the impact of different architectural choices.

The main contributions of this work are:

- Adapting the transformer model to handle the challenges of wind nowcasting data, including the ability to encode a context in a permutation-invariant way and generate forecasts in a non-autoregressive fashion.
- Demonstrating experimentally that the proposed transformer-based model is the best model for high-altitude wind prediction and for modeling other dynamical systems (Poisson equation and Darcy Flow equation)
- An in-depth examination of the differences between models, providing explanations for the impact of design choices such as latent representation bottlenecks on the final performance of the trained models.

## 2. Related works

The use of DL for weather nowcasting has gained popularity in recent years, with an increasing number of models being developed that match or surpass the performance of traditional PDE solving systems. The advantage of DL-based models is that they can leverage large amounts of data, resulting in improved performance with increasing data availability. Initially applied to precipitation nowcasting based on 2D radar images (Suman et al., 2021; Shi et al., 2017), DL-based models have recently demonstrated superiority over traditional methods for longer forecast periods (Lam et al., 2022). In the case of radar precipitation, data is organized as images, and convolutional neural networks are utilized. For 3D spherical grid data, graph neural networks are employed. However, in our study, the dataset is distributed sparsely along flight corridors, making these previously mentioned methods inapplicable.

The use of DL for dynamic system modeling, in general, has also seen recent advancements (Li et al., 2021; Gupta & Brandstetter, 2022; Pfaff et al., 2020) for similar reasons as in weather forecasting. However, most approaches in this field also typically operate on regularly-spaced data as well.

Neural Processes (Garnelo et al., 2018; Kim et al., 2019), Graph Element Networks (Alet et al., 2019) and Transformers (Vaswani et al., 2017) are three DL-based architectures that are capable of modeling general sets. In this study, we will conduct a comparison of these models by selecting a representative from each category. Additionally, Transformer

models have been previously adapted for set classification tasks (Lee et al., 2019), and here we adapt them to generate forecasts.

Pannatier et al. (2021) also examined wind data collected along flight trajectories to improve wind nowcasting, employing a kernel-based method. This method incorporates a distance metric with learned parameters to combine contexts for prediction in any spatial location. A major drawback of this technique is that the forecast is constrained to the convex hull of the input measures, which limits its ability. A comparison of our method with this approach and the different results can be found in the Appendix C.

## 3. Methodology

### 3.1. Dataset: Context and Targets

The problem addressed in this paper is the prediction of target values given a context and a prediction target position. Data is in the form of pairs of vectors  $(\mathbf{c}_x, \mathbf{c}_y)$  and  $(\mathbf{t}_x, \mathbf{t}_y)$  where  $\mathbf{c}_x$  and  $\mathbf{t}_x$  are the position and  $\mathbf{c}_y$  and  $\mathbf{t}_y$  are the measurements (or values). The positions lie in the same underlying space  $\mathbf{c}_x, \mathbf{t}_x \in \mathbb{X} \subseteq \mathbb{R}^D$ , but the context and target values need not necessarily belong to the same space. We define the corresponding spaces as  $\mathbf{c}_y \in \mathbb{I} \subseteq \mathbb{R}^E$  and  $\mathbf{t}_y \in \mathbb{O} \subseteq \mathbb{R}^F$ , respectively, where  $D, E, F$  are integers that need not be equal.

Here is how we adapted a dataset of wind speed measurement in a dataset corresponding to an extrapolating task. To accomplish this, we divide the dataset into time slices of approximately 1 minute and create pairs of sets with a delay in between, as illustrated in Figure 2. In this case, the context is made up of past wind speed, and the targets are wind speed measurements taken subsequently, possibly at different positions. The underlying space  $\mathbb{X}$  corresponds to the 3D Euclidean space, and both  $\mathbb{I}$  and  $\mathbb{O}$  are both wind speed measurements in the  $x, y$  plane. For the other synthetic cases and the ablation study, the dataset descriptions and corresponding spaces can be found in Table 5.

### 3.2. Models: Building blocks

All models considered for the extrapolation take as input a set of context pairs  $\{(\mathbf{c}_x, \mathbf{c}_y)_i\}_{i=1}^{N_c}$ , as well as target positions, denoted  $\{(\mathbf{t}_x)_i\}_{i=1}^{N_t}$ . These inputs are processed by an encoder which maps the context to a latent representation, and a decoder which takes the target positions as input and produces a predicted target value  $\{(\mathbf{t}_y)_i\}_{i=1}^{N_t}$  conditioned on the latent representation. The encoder should be permutation-invariant, while the decoder should be equivariant to permutations of the target positions. All models first process the context and target positions with a per-token multi-layer perceptron (MLP).

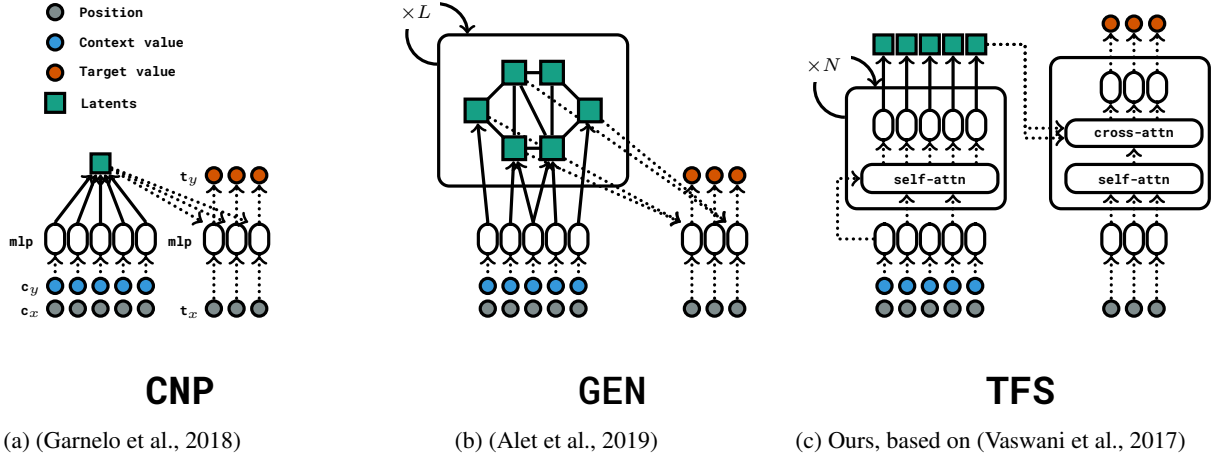


Figure 1: Illustration of the different models for modeling irregularly-spaced data compared in this work. Each model encodes a context ( $c_x, c_y$ ) in a position-invariant manner, then uses its latent representation to decode query position  $t_x$  into forecast  $t_y$ , where mlp is a per-token multilayer perceptron, self/cross-attn are self/cross-attention layers. GEN process the latents by applying  $L$  layer of message-passing. TFS have  $N$  encoder and decoder layers.

### 3.3. Transformer(s) (TFS, Ours)

Transformers enjoy several favorable properties. Compared to the alternatives, TFS maintains a single latent representation per input measurement, which conveys the ability to propagate gradients easily and correct errors in training quickly. TFS employs cross-attention to combine information from encoded latents. This forms a flexible and powerful method for approaching the latent space.

However, some modifications are necessary. Our TFS model adapts the transformer architecture (Vaswani et al., 2017) by incorporating several modifications.

Firstly, our TFS model does not use positional encoding for both the encoder and decoder. Since all feed-forward and normalization layers are applied per token and self-attention is invariant to the permutation of the input, this results in a permutation-invariant model. Secondly, we remove causal masking in the decoder, allowing each target feature to attend to all other targets and context measurements. Without the need for causal masking, TFS can generate all the output in one pass in a non-autoregressive way. Finally, we experimented with using encoders and decoders of different depths similarly to (Kasai et al., 2020), but as it did not substantially increase performance, we elected to use an equal number of layers.

### 3.4. Graph Element Network(s) (GEN)

Another model that we evaluate in this work is Graph Element Networks (GEN) (Alet et al., 2019), which utilizes a graph as a latent representation. The encoder maps measurements to the nodes of the graph based on their distance to the nodes, and the nodes' features are processed by  $L$  iteration of message passing. The node positions are additional parameters that must be initialized intelligently and whose update process is governed by stochastic gradient descent optimization. The edges of the graph govern the order of message passing and should be chosen carefully. The conditioning process involves concatenating the encoded targets with a weighted average of the latent vectors.

GEN inductive bias allows a single latent vector to summarize the information contained in a specific area of the space. This is a desirable property if one knows that the modeled phenomenon depends primarily on the neighboring states. Additionally, it includes a distance-based encoding and decoding scheme, which transformers must learn. However, the only way for the model to learn non-local patterns is through message passing.

### 3.5. Conditional Neural Process(es) (CNP)

CNP (Garnelo et al., 2018) are a subset of GEN. Specifically, a CNP is a GEN with a graph comprised of a single node and no message passing is performed. While CNP possess the desirable property of being able to model any permutation-invariant function (Zaheer et al., 2017), their

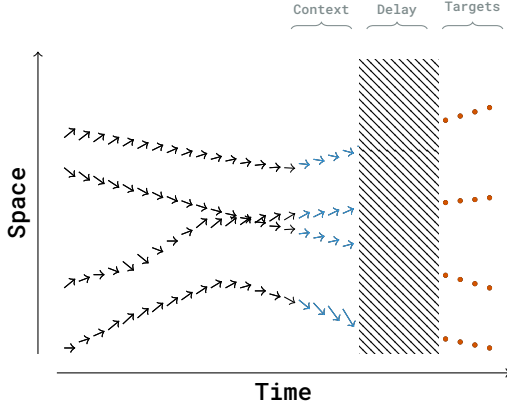


Figure 2: Description of the context and target sets in the wind nowcasting case. The context set and the target set are time slices separated by a delay, which corresponds to the forecasting window. The underlying space is in that case  $\mathbb{X} \subseteq \mathbb{R}^3$  and the context values and target values both are representing wind speed and belong to the same space  $\mathbb{I} = \mathbb{O} \subseteq \mathbb{R}^2$ .

expressive capability is constrained by the single node architecture (Kim et al., 2019). Despite this, CNP serve as a valuable baseline for comparison in the study of GEN and TFS and are considerably faster to train.

## 4. Experiments

We evaluate the models on the practical task wind nowcasting and then we show that they can be applied to various other tasks by tackling standard PDE modeling tasks. Finally, we conducted a series of ablation to motivate the use of our model.

### 4.1. High-altitude Wind Nowcasting

In this part, we present the results of our high-altitude wind nowcasting efforts. Our dataset, described in Section 3.1, consists of wind speed measurements collected by airplanes with a sampling frequency of four seconds, resulting in time slices containing between 50 and 1500 data points. We investigated the use of various time intervals and found that longer time slices did not improve forecast quality. The goal of our models is to predict wind conditions at various query points 30 minutes into the future. We evaluate performance using the Root Mean Square Error (RMSE) metric, as in previous work. The results of our models are shown in Table 1. We find that, despite theoretical limitations, the Gaussian Kernel Averaging (GKA) (Pannatier et al., 2021) model used in previous work still achieves good performance. We find that Transformer models are the only ones capable of achieving better performance in this setup. We outline the limitations of previous work in Appendix C.

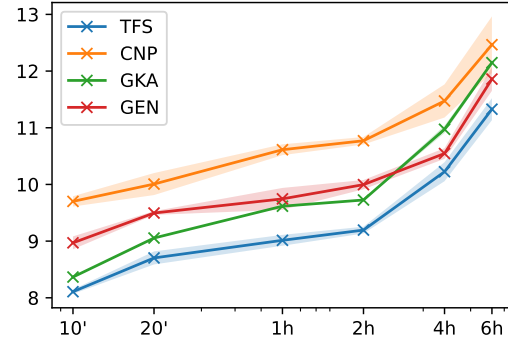


Figure 3: RMSE of the different models depending on the forecast duration (lower is better). We ran three experiments varying the pseudorandom number generator seeds for each time window and each model to measure the standard deviation. The error is not increasing drastically over the first two hours because the wind has some persistence and the context values are good predictors of the targets in that regime.

In addition, we evaluated the performance of our models as a function of forecast duration, as shown in Figure 3. We selected model configurations with approximately 100,000 parameters and ran each model using three different pseudorandom number generator seeds. Our results indicate that Transformer models consistently perform better than other models for any forecast duration. Furthermore, we observe that the GKA model performs well for short time horizons when most of the information in the context is still up-to-date. However, as the time horizon increases, the GKA model’s lack of flexibility becomes more apparent, and GEN becomes more competitive.

### 4.2. Poisson Equation

We evaluate the performance of various models on two synthetic tasks: modeling the Poisson equation on the dataset used in Alet et al. (2019) and the Darcy Flow equation on an adapted version of the dataset used in Li et al. (2021).

The Poisson equation models the case of a unit square with sources represented by  $\phi(x, y) \in \mathbb{R}$  and fixed boundary conditions  $\omega \in \mathbb{R}$ . The equation is given by:

$$\begin{cases} \Delta\phi(x, y) = \psi(x, y) & \text{if } (x, y) \in (0, 1)^2 \\ \phi(x, y) = \omega & \text{if } (x, y) \in \partial[0, 1]^2 \end{cases} \quad (1)$$

It should be noted that the boundary constant and sources function  $\phi(x, y)$  conditions can change for each sample.

The dataset used in (Alet et al., 2019) uses three dimensions for the context values  $\mathbf{c}_y \in \mathbb{I} \subseteq \mathbb{R}^3$ : either sources values  $\phi(x, y) = \mu$  inside the domain encoded as  $\mathbf{c}_x, \mathbf{c}_y =$

Table 1: Results of the High-Altitude Wind Nowcasting, Poisson equation and Darcy Flow equation. Each model ran for respectively 10, 2000, and 1000 epochs on an NVIDIA GeForce GTX 1080 Ti. The low number of epochs for wind nowcasting is due to the amount of data which is considerably larger than in the other experiments. The standard deviation is computed over 10 runs. We choose the configuration of the models so that every model has a comparable number of parameters. We underlying the best models for each size and we put in bold the best model overall.

Model	Size	Wind Nowcasting		Poisson Equation		Darcy Flow Equation	
		Train RMSE ( $\downarrow$ )	Val RMSE ( $\downarrow$ )	Train MSE ( $\downarrow$ )	Val MSE ( $\downarrow$ )	Train rel MSE ( $\downarrow$ )	Val rel MSE ( $\downarrow$ )
CNP	5k	11.94 $\pm$ 0.78	10.19 $\pm$ 0.21	.127 $\pm$ .0179	.130 $\pm$ .0134	.064 $\pm$ 0.0083	.070 $\pm$ 0.0067
	20k	10.19 $\pm$ 1.83	10.11 $\pm$ 0.20	.084 $\pm$ .0057	.105 $\pm$ .0012	.027 $\pm$ 0.0012	.042 $\pm$ 0.0004
	100k	10.17 $\pm$ 1.24	10.20 $\pm$ 0.26	.021 $\pm$ .0040	.105 $\pm$ .0024	.021 $\pm$ 0.0031	.043 $\pm$ 0.0006
GEN	5k	11.02 $\pm$ 3.19	9.84 $\pm$ 2.92	.011 $\pm$ .0006	.017 $\pm$ .0011	.022 $\pm$ 0.0006	.034 $\pm$ 0.0007
	20k	9.98 $\pm$ 0.76	9.24 $\pm$ 0.35	.006 $\pm$ .0006	.020 $\pm$ .0054	.022 $\pm$ 0.0013	.034 $\pm$ 0.0015
	100k	9.56 $\pm$ 0.21	9.23 $\pm$ 0.44	.011 $\pm$ .0122	.048 $\pm$ .0389	.022 $\pm$ 0.0024	.033 $\pm$ 0.0015
TFS (Ours)	5k	9.86 $\pm$ 0.21	8.75 $\pm$ 0.14	.022 $\pm$ .0021	.055 $\pm$ .0248	.025 $\pm$ 0.0005	.032 $\pm$ 0.0007
	20k	9.69 $\pm$ 0.38	8.70 $\pm$ 0.06	.005 $\pm$ .0008	.017 $\pm$ .0014	.022 $\pm$ 0.0016	.031 $\pm$ 0.0005
	100k	9.55 $\pm$ 0.19	<b>8.67<math>\pm</math> 0.07</b>	.001 $\pm$ .0001	<b>.016<math>\pm</math> .0045</b>	.023 $\pm$ 0.0013	<b>.030<math>\pm</math> 0.0005</b>

Table 2: Evaluation of the wind nowcasting task according to standard weather metrics [Appendix D]. The optimal value of the metric is denoted as indicated in the parenthesis. TFS is the best model overall, which has the lowest absolute error, but it tends to have a systematical bias along the  $y$  axis (rel BIAS) and output values that have a larger dispersion than GEN.

Model	RMSE ( $\downarrow$ )	angle MAE ( $\downarrow$ )	norm MAE ( $\downarrow$ )	rel BIAS x (0.0)	rel BIAS y (0.0)	rSTD (1.0)	NSE ( $\uparrow$ )
CNP	10.99 $\pm$ 0.75	25.55 $\pm$ 1.22	9.22 $\pm$ 0.33	0.00 $\pm$ 0.09	-1.09 $\pm$ 0.03	1.25 $\pm$ 0.07	-0.23 $\pm$ 0.01
GEN	8.97 $\pm$ 0.06	22.56 $\pm$ 0.77	6.97 $\pm$ 0.05	-0.02 $\pm$ 0.03	-0.97 $\pm$ 0.21	<b>1.09<math>\pm</math> 0.07</b>	0.25 $\pm$ 0.02
GKA	8.44 $\pm$ 0.01	<b>21.89<math>\pm</math> 0.02</b>	6.65 $\pm$ 0.02	-0.02 $\pm$ 0.00	-1.78 $\pm$ 0.02	1.13 $\pm$ 0.00	0.31 $\pm$ 0.01
TFS (Ours)	<b>7.99<math>\pm</math> 0.15</b>	22.17 $\pm$ 1.20	<b>6.48<math>\pm</math> 0.50</b>	0.08 $\pm$ 0.10	-2.21 $\pm$ 2.67	1.17 $\pm$ 0.04	<b>0.43<math>\pm</math> 0.08</b>

$(x, y)$ ,  $(\mu, 0, 0)$  or boundary conditions  $\phi(x, y) = \omega$  on the boundaries, encoded as  $\mathbf{c}_x, \mathbf{c}_y = (x, y), (0, \omega, 1)$ . The target space is one-dimensional  $\mathbf{t}_y \in \mathbb{O} \subseteq \mathbb{R}$  and corresponds to the solution of the Poisson equation at that point. Additional details about the setup can be found in the Appendix A.2.

We ran all models for three different sizes on this particular setup and found that in this setup TFS reaches similar accuracies to GEN while suffering less from overfitting. We initialized GEN with a  $7 \times 7$  regularly initialized grid on the  $[0, 1]^2$  as in the original work (Alet et al., 2019).

### 4.3. Darcy Flow Equation

We evaluated the performance of various models in solving the Darcy Flow equation on the unit grid with null boundary conditions, as described in (Li et al., 2021). Specifically, we aimed to predict the value of the function  $u$ , given the diffusion function  $a$ , with the two related implicitly through the PDE given by:

$$\begin{cases} -\nabla \cdot (a(x)\nabla u(x)) = 1 & \text{if } x \in (0, 1)^2 \\ u(x) = 0 & \text{if } x \in \partial[0, 1]^2. \end{cases} \quad (2)$$

The dataset used in our study was adapted from that used

in (Li et al., 2021), and originally generated by a traditional high-resolution PDE solver. The dataset consisted of a  $1024 \times 1024$  grid, which was subsampled uniformly at random and arranged into context-target pairs. The context is comprised of the evaluations of the diffusion coefficient:  $(\mathbf{c}_x, \mathbf{c}_y) = ((x, y), a(x, y))$ , and the target is the solution of the Darcy Flow equation at a position,  $(\mathbf{t}_x, \mathbf{t}_y) = ((x, y), u(x, y))$ .

The results are presented in Table 1, they are coherent with the rest of the experiment and show that the TFS model is able to outperform all the other considered models. We used the same initialization for GEN than in the Poisson Equation.

## 5. Understanding failure modes

We examine here the limitations of CNP latent representation for encoding a context. Specifically, we focus on the bottleneck effect that arises from using a single vector to encode the entire context, resulting in an underfitting problem (Garnelo et al., 2018; Kim et al., 2019). To address this issue, we propose three simple experiments. (1) We show in which case baselines are not able to retrieve information in the context that they use for conditioning, and why TFS are not suffering from this problem. (2) We show that maintain-

ing disentangled latent representation helped to the correct attribution of perturbations. (3) We show that this improved latent representation leads to better error correction.

### 5.1. Context information retrieval

Every model considered in this work encodes context information in a different manner. Ideally, each should be capable of using or retrieving every measure in their context. We will see that excessive bottlenecking in the latent space can make this difficult or impossible.

To demonstrate this result, we design a simple experiment in which each model encodes a set of 64 measures ( $\mathbf{c}_x, \mathbf{c}_y$ ), and the decoder is then tasked with retrieving the corresponding  $\mathbf{c}_y$  given the  $\mathbf{c}_x$ . We train all models on this task using Mean-Square Error (MSE) as a loss function. For this task, the models differ only in their latent representation: they all use a distance-based conditioning function and a one-layer decoder. The training and validation set have respectively 10.000 and 1.000 pair of sets of 64 examples.

It is worth noting that the models have access to all the information they need to solve the task with near-zero MSE. We conducted several experiments, starting by randomly sampling 2D context positions  $\mathbf{c}_x = (x, y)$  from a Gaussian distribution and computing the associated deterministic smooth function:

$$\mathbf{c}_y = \sin(\pi f x) \cos(\pi f y) \in \mathbb{R} \quad (3)$$

where  $f$  is a frequency parameter that governs problem difficulty. The higher  $f$  is, the more difficult the function becomes, as local information becomes less informative about the output.

The results of this experiment, presented in Figure 4, show that CNP and GEN fail to effectively learn this task when the frequency is high enough. We ascribe this to a failure to distinguish context measures that are close in the underlying space but have different values caused by insufficient flexibility in the latent space.

In contrast, models with disentangled latent representations, such as TFS, can effectively learn the task. To further demonstrate this specific difference between TFS and GEN, we created two hybrid models. The first one denoted GNG (for *GEN no graph*), is adapted from GEN but maintains one node per measure. Edges are artificially added between neighboring measures which serve as the base structure for  $L$  steps of message-passing. This latent representation is computationally expensive as it requires the creation of a graph per set of measurements, but it does not create a bottleneck in the latent representation. We found that GNG is indeed able to learn the task at hand. We then followed the reverse approach and artificially added a bottleneck in the la-

tent representation of transformers by using Perceiver Layer (Jaegle et al., 2021) with  $P$  learned latent vectors instead of the standard self-attention in the transformer encoder (and call the resultant model *PER*). When  $P$  is smaller than the number of context measurements, it creates a bottleneck and PER does not succeed in learning the task.

If the underlying space is smooth enough, GEN and CNP are capable of reaching perfect accuracy on this task as they can rely on neighboring values to retrieve that information. They even in some cases, reach zero error faster than their disentangled counterparts.

This experiment demonstrates that TFS can use its disentangled latent representations, to efficiently retrieve context information regardless of the level of discontinuity in the underlying space, while models with bottlenecks, such as CNP and GEN, are limited in this regard and perform better when the underlying space is smooth.

TFS	0	0	0	0	0	0
GNG	0	0	0	0	0	0
PER	0	0	0.01	0.01	0.01	0.05
GEN	0	0	0.05	0.07	0.07	0.22
NP	0	0	0.18	0.22	0.22	0.80
	$f=0.1$	$f=1.0$	$f=10$	$f=100$	$f=1000$	Random

Figure 4: Results of the information retrieval experiment. The two first rows correspond to models with no bottlenecks. The x-axis corresponds to datasets created with increasing frequency. When the learned function does not vary too much spatially, models with bottlenecks can suffice. GEN is using again a  $7 \times 7$  grid initialization in that setup. The models in italics represent hybrid architectures: *GNG* = GEN without a graph, which maintains a latent per context measure and *PER* = transformer with a perceiver layer (Jaegle et al., 2021) which creates a bottleneck.

### 5.2. Correct perturbation attribution

We next examine the ability of disentangled latent representations to more efficiently correct errors during training.

Specifically, we ask whether models can correctly attribute the effects of a perturbation in the output to backpropagation.

We use TFS and GEN models applied to the information retrieval task from the previous section. We pre-train each model to zero error on the validation data in a smooth case ( $f = 1.0$ ), and then apply a perturbation  $\gamma$  on one of the output values, compute the loss between the perturbed output and the one without perturbation and backpropagate it through each model. The norm of gradients corresponding to the latent at the last encoder layer is shown in Figure 5. We see that TFS only receives a signal on the corresponding latent while the other models receive signals on different latents.

We hypothesize that this spread of gradients to other non-related latents causes problems during training, as the models need to adjust all parameters to correct the artificial error while maintaining the same value for the other output values. Models with a disentangled representation do not suffer from this problem as they can update the corresponding latent independently.

To further demonstrate this property, for the models described above, we tabulate the number of backpropagation passes needed to fully correct the artificial error on one output (to reach a zero error on the validation set again). The results are shown in Figure 6. We used TFS as a reference and observed that all models with an entangled representation required more time to reach a zero error on the validation set. We found that the more entangled the representation, the more time was needed to reach the desired performance. Note that, in this setup, GEN  $1 \times 1$  is equivalent to CNP.

These experiments demonstrate that models with disentangled latent representations can more efficiently correct errors during training, while models with entangled representations struggle to do so and require more time to reach the desired performance.

### 5.3. Decoder and conditioning function

GEN and TFS differ not only in their latent representation but also on two other points: (1) the way that they access the encoded information in the decoder and (2) how much computing power is used in the decoder stack.

In all three models, we tried using either a distance-based function or cross-attention to combine the target position with the encoded latents. CNP concatenate the same context vector to all target queries, which we model as equivalent to averaging the latents based on the distance in the case that there is only one latent.

Specifically, each latent is associated with a position  $\mathbf{l}_x$  in the underlying space with corresponding value  $\mathbf{l}_y$ . Condi-

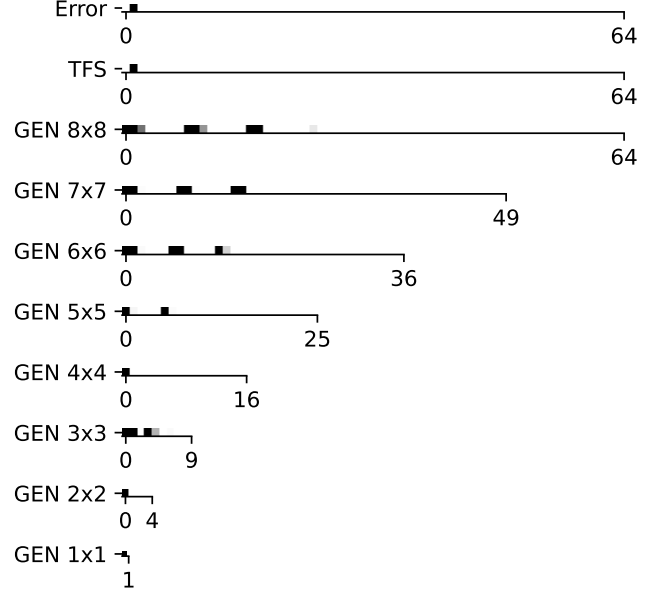


Figure 5: Gradients on the last layer of the encoder corresponding to a sufficiently large artificial error of  $\gamma = 10.0$  added to the second output. As can be observed, TFS maintains a disentangled representation and the gradient at that layer is non-zero only on the corresponding latent. We compared it to different GEN each initialized with a graph corresponding to a regular grid of size  $i \times i$  with  $i \in \{1, \dots, 8\}$ . Due to the bottleneck effect, the gradients corresponding to one error are propagated across different latent vectors in the case of GEN. Even when there are enough latents (case GEN  $8 \times 8$ ), GEN still suffer from this problem as they use a distance-based conditioning function that does not allow for a one-to-one mapping between targets and latents.



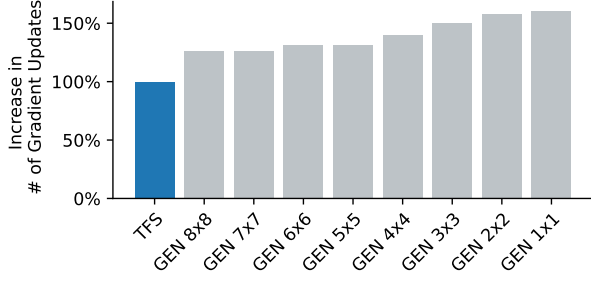


Figure 6: Comparison of the number of gradient updates required to correct an artificial error, with respect to TFS (lower is better). The y-axis represents the increase in percentage in the number of steps required to reach a perfect accuracy with respect to TFS as reference. We compared TFS to different GEN each initialized with a graph corresponding to a regular grid of size  $i \times i$  with  $i \in \{1, \dots, 8\}$ . It can be observed that all GEN take more steps to correct the same mistake, and the more entangled the latent representation is, the more time it requires to correct the problem.

tioning is made by averaging the latent features based on their distance with the query  $\mathbf{t}_x$ . Its formula is given by:

$$z = \sum_{\mathbf{l} \in \text{latents}} r(\text{dist}(\mathbf{l}_x, \mathbf{t}_x)) \mathbf{l}_y \quad (4)$$

Where  $r : \mathbb{R} \rightarrow [0, 1]$  is a function that maps distances to weights, and  $\mathbf{l}_x$  represents the position associated with the latent nodes with value  $\mathbf{l}_y$ . This vector  $z$  is then concatenated to the target position  $\mathbf{t}_x$  and fed to the decoder which is a MLP in this case.

GEN use this distance-based aggregation function by default whereas TFS uses cross-attention. We tried using cross-attention for CNP and GEN and using the same distance-based aggregating function for TFS using the distance between context position and target position as a reference for this scheme. For GEN and CNP using cross-attention give approximately the same results, but using distance-based conditioning for TFS hurts the performance significantly.

We also ran ablations that created hybrid cases for both transformers and GEN and concluded that adding decoding layers helped TFS to reach better performance. Adding layers to the GEN decoder drastically reduces model performance, which seems to be coherent with the fact that GEN were shown to be more prone to overfitting in the results section.

Table 3: Results of the ablation of the conditioning function used to combine the latents with the target position. We adapted the architecture so that they used both a distance-based conditioning function, which combines the query position with a weighted average of the nearest latents and standard cross-attention. We show in italics hybrid architecture where we had to switch the default conditioning method. For GEN and CNP replacing the conditioning method does not impact the performance, but for TFS switching to a distance-based conditioning function impacts the performance drastically.

Model	Distance-based	Cross-attention
CNP	.115 ± .015	<i>.119 ± .014</i>
GEN	.024 ± .004	<i>.022 ± .006</i>
TFS	<i>.042 ± .023</i>	<b>.020 ± .011</b>

Table 4: Results of the decoder-layer ablation. One difference between TFS and GEN is that by default TFS use multiple layers in its decoder whereas GEN uses one, and delegates all processing to the encoder. We see that having multiple decoder layers helps the transformer whereas it impacts the performance of the GEN.

Model	# Decoder layers		
	1	2	4
GEN	.021 ± .002	.040 ± .012	.106 ± .004
TFS	.020 ± .011	.019 ± .005	<b>.013 ± .001</b>



## 6. Conclusion

In this work, we adapted a transformer model to handle the challenges of wind nowcasting data, including the ability to encode a context in a permutation-invariant way and generate forecasts in a non-autoregressive way. We demonstrated that the proposed transformer-based model was able to reach the best performance for high-altitude wind prediction and for other dynamical systems (Poisson equation and Darcy Flow equation). We then explained why Transformers were capable of outperforming other models on that task and provided an in-depth examination of the differences between models, providing explanations for the impact of design choices such as latent representation bottlenecks on the final performance of the trained models.

Transformers condition predictions on different types of information, such as topography, or other weather forecasting source. Likely, this will enable further improvements to the quality of our model predictions. These perspectives might be part of future work.

**Acknowledgement** Arnaud Pannatier was supported by the Swiss Innovation Agency Innosuisse under grant number 32432.1 IP-ICT – “MALAT: Machine Learning for Air Traffic.” Kyle Matoba was supported by the Swiss National Science Foundation under grant number FNS-188758 “CORTI”.

## References

- Alet, F., Jeewajee, A. K., Villalonga, M. B., Rodriguez, A., Lozano-Perez, T., and Kaelbling, L. Graph element networks: adaptive, structured computation and memory. In *International Conference on Machine Learning*, pp. 212–222. PMLR, 2019.
- Garnelo, M., Rosenbaum, D., Maddison, C., Ramalho, T., Saxton, D., Shanahan, M., Teh, Y. W., Rezende, D., and Eslami, S. M. A. Conditional neural processes. In Dy, J. and Krause, A. (eds.), *Proceedings of the 35th International Conference on Machine Learning*, volume 80 of *Proceedings of Machine Learning Research*, pp. 1704–1713. PMLR, 10–15 Jul 2018. URL <https://proceedings.mlr.press/v80/garnelo18a.html>.
- Ghiggi, G., Humphrey, V., Seneviratne, S. I., and Gudmundsson, L. Grun: an observation-based global gridded runoff dataset from 1902 to 2014. *Earth System Science Data*, 11(4):1655–1674, 2019. doi: 10.5194/essd-11-1655-2019. URL <https://essd.copernicus.org/articles/11/1655/2019/>.
- Gupta, J. K. and Brandstetter, J. Towards multi-spatiotemporal-scale generalized pde modeling, 2022. URL <https://arxiv.org/abs/2209.15616>.
- Jaegle, A., Borgeaud, S., Alayrac, J.-B., Doersch, C., Ionescu, C., Ding, D., Koppula, S., Zoran, D., Brock, A., Shelhamer, E., et al. Perceiver io: A general architecture for structured inputs & outputs. *arXiv preprint arXiv:2107.14795*, 2021.
- Kasai, J., Pappas, N., Peng, H., Cross, J., and Smith, N. A. Deep encoder, shallow decoder: Reevaluating the speed-quality tradeoff in machine translation. *CoRR*, abs/2006.10369, 2020. URL <https://arxiv.org/abs/2006.10369>.
- Kim, H., Mnih, A., Schwarz, J., Garnelo, M., Eslami, A., Rosenbaum, D., Vinyals, O., and Teh, Y. W. Attentive neural processes. In *International Conference on Learning Representations*, 2019. URL <https://openreview.net/forum?id=SkE6PjC9KX>.
- Lam, R., Sanchez-Gonzalez, A., Willson, M., Wyrnsberger, P., Fortunato, M., Pritzel, A., Ravuri, S., Ewalds, T., Alet, F., Eaton-Rosen, Z., Hu, W., Merose, A., Hoyer, S., Holland, G., Stott, J., Vinyals, O., Mohamed, S., and Battaglia, P. Graphcast: Learning skillful medium-range global weather forecasting, 2022. URL <https://arxiv.org/abs/2212.12794>.
- Lee, J., Lee, Y., Kim, J., Kosiorek, A. R., Choi, S., and Teh, Y. W. Set transformer. In *International Conference on Machine Learning*, 2019.
- Li, Z., Kovachki, N. B., Azizzadenesheli, K., Liu, B., Bhattacharya, K., Stuart, A., and Anandkumar, A. Fourier neural operator for parametric partial differential equations. In *International Conference on Learning Representations*, 2021. URL <https://openreview.net/forum?id=c8P9NQVtmnO>.
- Pannatier, A., Picatoste, R., and Fleuret, F. Efficient wind speed nowcasting with gpu-accelerated nearest neighbors algorithm, 2021. URL <https://arxiv.org/abs/2112.10408>.
- Pfaff, T., Fortunato, M., Sanchez-Gonzalez, A., and Battaglia, P. Learning mesh-based simulation with graph networks. In *International Conference on Learning Representations*, 2020.
- Shi, X., Gao, Z., Lausen, L., Wang, H., Yeung, D.-Y., Wong, W.-k., and Woo, W.-c. Deep Learning for Precipitation Nowcasting: A Benchmark and A New Model. *Advances in Neural Information Processing Systems*, 2017.
- Suman, R., Karel, L., Matthew, W., Dmitry, K., Remi, L., Piotr, M., Megan, F., Maria, A., Sheleem, K., Sam, M., Rachel, P., Amol, M., Aidan, C., Andrew, B.,

Karen, S., Raia, H., Niall, R., Ellen, C., Alberto, A., and Shakir, M. Skilful precipitation nowcasting using deep generative models of radar. *Nature*, 597(7878): 672–677, 09 2021. ISSN 1476-4687. doi: 10.1038/s41586-021-03854-z. URL <https://doi.org/10.1038/s41586-021-03854-z>.

Vaswani, A., Shazeer, N., Parmar, N., Uszkoreit, J., Jones, L., Gomez, A. N., Kaiser, Ł., and Polosukhin, I. Attention is all you need. *Advances in neural information processing systems*, 30, 2017.

Zaheer, M., Kottur, S., Ravanbakhsh, S., Póczos, B., Salakhutdinov, R., and Smola, A. J. Deep sets. *CoRR*, abs/1703.06114, 2017. URL <http://arxiv.org/abs/1703.06114>.

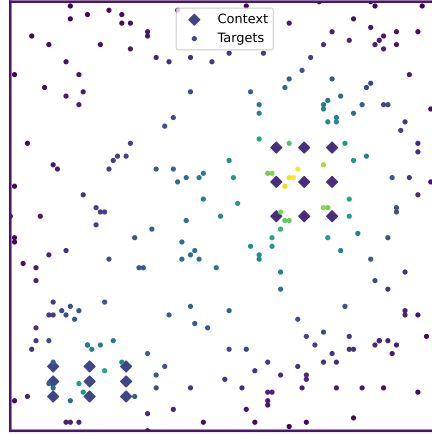


Figure 7: A sample of the Poisson equation dataset (Alet et al., 2019). • represents the targets, The context values are comprised of points on the boundaries and points on the sources and sink are represented by ♦ which corresponds to their thermal coefficient.

## A. Dataset descriptions

### A.1. Wind nowcasting

This part uses the same dataset as Pannatier et al. (2021). It is available here: <https://zenodo.org/record/5074237>. The corresponding task is important for ATC: predicting wind at high altitudes using the live measures broadcasted by airplanes is mandatory to be able to manage the air space efficiently. Here, the underlying space is European airspace,  $\mathbb{X} \subseteq \mathbb{R}^3$ . In particular, for the  $z$  direction, most of the values are recorded at high altitudes, between 4,000 and 12,000m. At these altitudes, ground-based measurements are not available and we must rely on measurements taken by airplanes themselves. As planes do not record the wind in the  $z$  direction, the input space corresponds to wind speed in the  $x, y$  plane  $\mathbb{I} \subseteq \mathbb{R}^2$ , and the output space is the wind speed measured later,  $\mathbb{O} \subseteq \mathbb{R}^2$ . In this particular setup, the models need to extrapolate in time, based on a set of the last measurements.

Airplanes measure wind speed with a sampling frequency of four seconds. We split the dataset into time slices, where each slice contains one minute of data, such that each time slice contains between 50 and 1500 data points. We tried different time intervals but noticed that having a longer time slice did not improve the quality of the forecasts. The objective for the different models is to output a prediction of the wind at different query points 30 minutes later.

### A.2. Poisson Equation

This section uses the same dataset as (Alet et al., 2019). It is available at [https://github.com/FerranAlet/graph\\_element\\_networks/tree/master/data](https://github.com/FerranAlet/graph_element_networks/tree/master/data)

Problem data is in the form of a mixed boundary condition: the temperature at the boundaries is a prescribed constant, the interior of the house is a small number of constant inhomogeneities, and all other interior points obey the Laplace Equation (1). A deep learning model is trained to predict the scalar-valued temperature function over the two-dimensional unit cube given the input data, and ground truth data in the form of  $(x, y, \text{temperature})$  tuples evaluated at arbitrary input points. A sample is depicted in Figure 7.

### A.3. Darcy Flow

This part adapts the dataset available in (Li et al., 2021). It is available at [https://github.com/neural-operator/fourier\\_neural\\_operator](https://github.com/neural-operator/fourier_neural_operator) and can be processed with the code given to rearrange it in

**Transformer-based Wind Nowcasting: Improving Performance with Disentangled Latent Representations**

Dataset	dim( $\mathbb{X}$ )	dim( $\mathbb{I}$ )	dim( $\mathbb{O}$ )	# Train. points	# Val. points	URL
Wind Nowcasting	3	2	2	26.956.857	927.906	(Pannatier et al., 2021) Dataset page
Poisson Equation	2	3	1	409.600	102.400	(Alet et al., 2019) Github Repository
Darcy Flow Equation	2	1	1	409.600	102.400	(Li et al., 2021) Github Repository
Random	2	1	1	640.000	64.000	Randomly generated
Sine	2	1	1	640.000	64.000	Randomly generated

Table 5: Description of the different datasets used in this study.

the irregular setup.

## B. Attention matrix for Wind Nowcasting

For all models, we can plot the norm of the input gradients to see how changing a given value would impact the prediction [Figure 8]. We see that Transformers seem to find a trade-off between taking into account the neighboring nodes and the global context.

## C. Flaws of the previous methods

Smart averaging strategies such as GKA are limited by design to the range of the values in their context. However, these baselines are useful as they are not prone to overfitting and in the case of time series forecasting (if the underlying variable has some persistence), the last values would in general be the best predictor of the next value. We hypothesize that over sufficiently short horizons, these methods would achieve performance similar to that from more complicated models, but when the prediction horizon rises, this design limitation would become more pronounced.

Since, for extrinsic forecasting, target points need not lie in the convex hull of context points, the greater flexibility of Transformers can make correct forecasts that are impossible with GKA. Figure 9a demonstrates this fact, with a plot of the target variable, the context points and the context convex hull in wind speed space.

But greater capacity means also more failure modes. As we saw in the results Table 2, Transformer is the only model to outperform GKA whereas other models, even if they are more flexible, fail to beat this baseline. On average 27% of the predictions were outside the convex hull of the context. In Figure 9c we analyze the percentage of measurements outside the convex hull produced by the different models. We can see that GKA is limited whereas the other models can compensate and predict values outside the convex hull.

## D. Wind nowcasting metrics

This section defines the metrics used for wind nowcasting.

**Root Mean Square Error (RMSE)** It takes the square root of the square distance between the prediction and the output. It has the advantage of having the same units as the forecasted values.

$$\text{RMSE}(\hat{t}, t) = \sqrt{\frac{\sum_k^N (\hat{t}_k - t_k)^2}{N}} \quad (5)$$

**Mean Absolute Error for angle (angle MAE)** It is interesting and sometimes more insightful to decompose the error made by the models in their angular and norm components. This is the role of this metric and the following.

$$\text{angle MAE}(\hat{t}, t) = \|(\alpha(\hat{t}) - \alpha(t))\|_{L_1} \quad (6)$$

where  $\alpha\left(\vec{x} = \begin{pmatrix} x \\ y \end{pmatrix}\right) = \arctan(y, x) * \frac{360}{2\pi}$

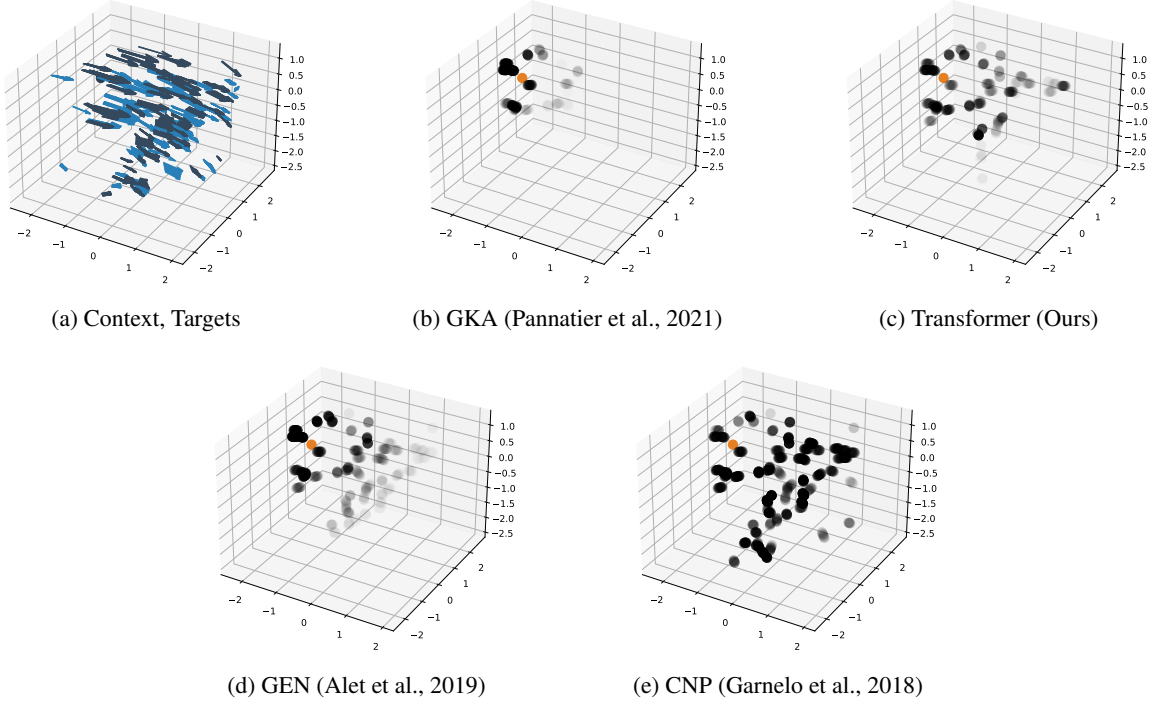


Figure 8: Displaying the importance given to points in the context to do the prediction for the different models for a given query point (orange). We used the norm of the input gradients for that purpose and highlight the context values that have the largest gradient with respect to the output. The opacity of the dots corresponds to the relative magnitude of the input gradients compared to other points in the context.

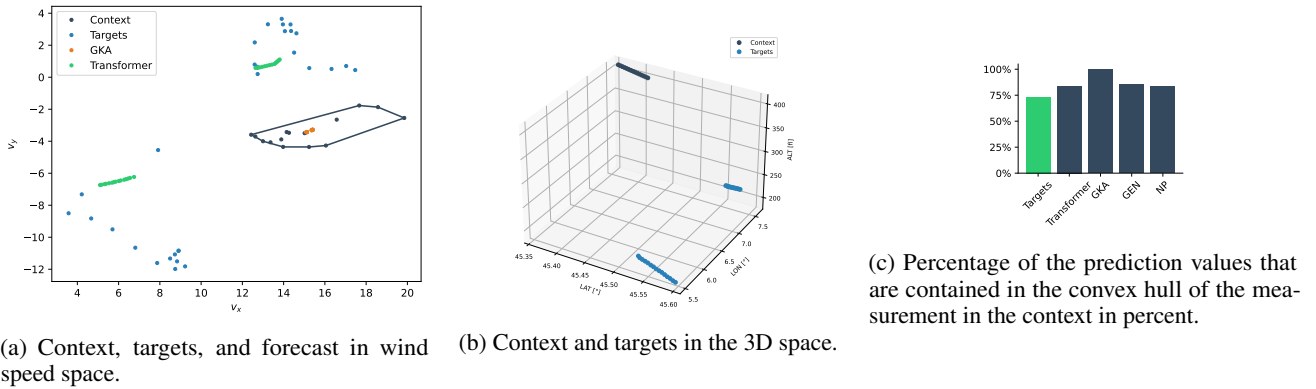


Figure 9: Context and the targets in wind speed and 3D space. Both are 1min slices of data. The targets are wind measurements recorded 30min after the one in the context. The forecasts of the Transformer model and the GKA model are plotted as well. GKA is restricted to predict within the convex hull of context values (depicted here in grey). Transformers do not suffer from this limitation.

**Mean Absolute Error for norm (norm MAE)** Following the explanation of the last paragraph:

$$\text{norm MAE}(\hat{t}, t) = \sum_k | \|\hat{t}_k\|_2 - \|t_k\|_2 | \quad (7)$$

**Relative Bias (rel BIAS) x,y** Additionally, we used weather metrics as in (Ghiggi et al., 2019). The relative bias measure if the considered model under or overestimate one quantity. It is defined as:

$$\text{rel BIAS}(\hat{t}, t) = \frac{\text{mean}(\hat{t}_k - t_k)}{\text{mean}(\hat{t}_k)} \quad (8)$$

**Ratio of standard deviation (rSTD)** The ratios of standard deviation indicate whether the dispersion of the output of the model matches the target distribution. It has an optimal value of 1.

$$\text{rSTD}(\hat{t}, t) = \frac{\text{std}(\hat{t})}{\text{std}(t)} \quad (9)$$

**NSE** The last domain metric used is the Nash-Sutcliffe efficiency (NSE), which compares the error of the model with the average of the target data. A score of 1 is ideal and a negative score indicates that the model was worse than the average prediction on average.

$$\text{NSE}(\hat{t}, t) = 1 - \frac{\text{MSE}(\hat{t}, t)}{\text{MSE}(t, \text{mean}(t))} \quad (10)$$